Peptide-Functionalized Layer-by-Layer Nanoparticles Demonstrate Improved Blood Brain
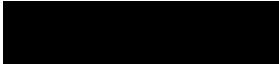Barrier Permeability for Glioblastoma Treatment

by

Priya Ganesh

Submitted to the Department of Materials Science and Engineering
in Partial Fulfillment of the Requirements for the Degree of Bachelor of Science at the
Massachusetts Institute of Technology – June 2023

Signature of Author .... ‌ ....

Priya Ganesh
Department of Materials Science and Engineering
May 10, 2023

Certified by .... ‌ ..

Paula Hammond
Thesis Supervisor
Professor of Chemical Engineering

.... ‌

Aristide Gumyusenge
Thesis Reader
Assistant Professor of Materials Science and Engineering

Accepted by ....

James LeBeau
Associate Professor of Materials Science and Engineering
Chair, DMSE Undergraduate Committee

Peptide-Functionalized Layer-by-Layer Nanoparticles Demonstrate Improved Blood Brain Barrier Permeability for Glioblastoma Treatment

Priya Ganesh, Candidate for B.S. in Materials Science and Engineering, Massachusetts Institute of Technology

Thesis Advisor: Prof. Paula Hammond, Department of Chemical Engineering

Thesis Reader: Prof. Aristide Gumyusenge, Department of Materials Science and Engineering

Abstract:

The greatest obstacle in the treatment of glioblastomas is the blood-brain barrier (BBB), the endothelial cells that line the vessels of the brain and are stitched together into a barrier by tight junction complexes. One approach to overcoming this barrier is encapsulating drugs in nanoparticles whose surfaces are engineered (usually, with the addition of ligands) to promote binding to various receptors of the BBB, thus triggering transcytosis and allowing the nanoparticle and its drug contents to cross the BBB. Previous research has shown that electrostatic absorption (as opposed to covalent functionalization) is a quick and effective method for attaching cationic, tumor-penetrating peptides to anionic nanoparticles synthesized through an iterative layer-by-layer (LbL) approach.

Here, I demonstrate that LbL nanoparticles functionalized with Angiopep-2, a BBB-penetrating peptide, can penetrate the BBB to deliver their contents to the brain. Peptide-functionalized particles were screened in an *in vitro* transwell model of the blood-brain barrier, and particularly promising candidates were screened in a mouse model through intravital imaging, leading to a conclusion that the combination of a poly-L-aspartate outer layer and Angiopep-2 leads to significant improvement in nanoparticle uptake in the brain. Future work will include *in vivo* experiments with peptide-functionalized LbL nanoparticles with a hyaluronic acid (HA) outer layer, as HA particles have been shown to have *in vivo* transport properties not reflected in *in vitro* transport experiments.[1]

Table of Contents

Chapter 1: Introduction and Literature Review

Glioblastoma multiforme (GBM) is an aggressive brain tumor that accounts for more than 60% of all brain and central nervous system tumors.[2] The current standard of care (surgical resection of the tumor followed by radiotherapy and chemotherapy) gives a median survival of only 15 months, so there is a significant need for improved therapies for glioblastomas.[3] The greatest obstacle in the delivery of cancer therapeutics to glioblastomas is the blood-brain barrier (BBB), or the lining of the blood vessels of the brain. Consisting primarily of a collection of endothelial cells that are stitched together into a barrier by tight junction complexes, the BBB is designed to prevent pathogens and other foreign objects from entering the brain. The inability of the BBB to distinguish between harmful substances and therapeutics leads to a fundamental problem in brain drug delivery: at least 95% of recently discovered candidate therapies are unable to enter the brain.[4] The need to develop drug delivery carriers for these therapies that are capable of crossing the BBB is clear and urgent.

A possible strategy for improving drug delivery is temporarily increasing the overall permeability of the BBB (e.g. through introducing small doses of vascular endothelial growth factor).[5] While this approach accomplishes the goal of allowing chemotherapeutics into the brainspace, unwanted pathogens and other chemicals can also enter the brain, since the BBB will be unable to function as required. Avoiding this problem, another approach is encasing the drugs in nanoparticles whose surfaces are engineered to promote binding to various receptors of the BBB. This binding triggers transcytosis (the receptor-mediated mechanism by which particles are transported across a cell), allowing the nanoparticle and its drug cargo to cross the BBB. This approach has been implemented widely in the literature. Polymeric nanoparticles, including those composed of poly (lactide-*co*-glycolic) acid (PLGA),[6] poly(ethylene imine),[7] and

poly(allylamine) hydrochloride,[8] have been shown to improve delivery efficiency for treatments of Alzheimer's and other neurological diseases. Liposomes, or spherical nanoparticles consisting of lipid bilayers, are often used to deliver gene therapies or chemotherapeutics, including doxorubicin, erlotinib, and paclitaxel, to brain cancers.[9] Other delivery carriers include dendrimers, micelles, and a variety of inorganic nanocarriers.[9] At this time, none of these carriers have advanced through clinical trials for glioblastoma treatment for a variety of reasons, including poor accumulation in the brain.

Often, nanocarriers are modified with ligands to promote uptake by certain endothelial cell protein receptors or sialic acid-containing glycosphingolipids called gangliosides.[10] One class of ligands that promote uptake by endothelial cells in the brain are BBB-penetrating "shuttle" peptides, which enable any attached cargo to cross the BBB without damaging it.[11] A number of known BBB shuttle peptides and their receptor targets can be found in the literature, including Angiopep-2 (LRP1 receptor), RAP12 (LRP1 receptor), B6 (Tf1 receptor), G23 (GM1 ganglioside), and RVG29 (nAchR receptor).[12–16] Angiopep-2, a 2.4 kDa, 19 amino acid, cationic (+2 at physiological pH) peptide, is the most widely-used BBB shuttle peptide; it has been conjugated to small molecules, polymeric nanoparticles, liposomes, dendrimers, and even nanotubes to improve transport across the BBB.[10,17] In all of these cases, Angiopep-2 is covalently linked to the cargo through a variety of chemistries, including EDC/NHS and cysteine/maleimide reactions.[18–20] While the resulting nanoparticles exhibit improvement in transport across the BBB, conjugation efficiency of the Angiopep-2 to the particle is generally low; Wang et al. report 50% conjugation efficiency and Figueiredo et. al. report 24% conjugation efficiency with EDC/NHS chemistry.[19,21] Luo et al. report 89% conjugation efficiency with cysteine/maleimide chemistry, but only load 0.014 mg peptide per mg nanoparticle.[22] In addition,

covalent conjugation often requires harsh chemicals, so lengthy dialysis purification is needed before the peptide-conjugated nanoparticles can be placed into the body. Here, we explore electrostatic adsorption of BBB shuttle peptides onto nanoparticles as a quick method for improving peptide loading and conjugation efficiency.

In this work, I draw upon the layer-by-layer (LbL) nanoparticle platform for drug delivery, which has been well-characterized by members of the Hammond Lab as well as others.[23–27] This platform involves sequentially electrostatically adsorbing ("layering") charged polymers onto oppositely charged nanoparticles. Often, chains of repeated charged amino acids are used as the charged polymers in this platform due to their simplicity and biocompatibility. Other biopolymers, like sodium hyaluronate, or polymers known to be biologically inert, such as poly(acrylic acid) are also common. Previously, Boehnke et al. demonstrated that electrostatic absorption (as opposed to covalent functionalization) is a quick and effective method for attaching cationic, tumor-penetrating peptides to anionic nanoparticles synthesized through an LbL approach.[28] These peptides were chosen specifically to target tumor cells in high grade serous ovarian cancer.[1] It was demonstrated that one of two cationic peptides tested did not impact the stability of the particle under purification and physiological salt conditions.[1] Only one of the four peptide-outer layer combinations demonstrated statistically significant improvement in nanoparticle-cell association when compared to the peptide-free particles, but it was hypothesized that this could be due to unique properties of the selected outer layers and that peptides might still improve intracellular nanoparticle trafficking.[1]

In this work, I aimed to construct a similar series of peptide-functionalized nanoparticles targeted to the BBB. The nanoparticle core is a fluorescently-labeled anionic liposome, consisting of phospholipids and cholesterol. Poly-L-arginine (PLR), a cationic poly-amino acid

that has been demonstrated to assist with endosomal escape of the nanoparticle, is then electrostatically adsorbed to the core until the particle is fully charge-converted (zeta potential > 30 mV).[27] Next, a polyanion layer is adsorbed until the particle's outer surface is negatively-charged (zeta potential < -30 mV) (we use poly-L-aspartate (PLD) and hyaluronic acid (HA) to probe the effect of outer layer chemistry on transport across the BBB both *in vitro* and *in vivo*). Finally, cationic BBB-penetrating peptides are adsorbed to the surface, although charge conversion is not achieved; the peptide-functionalized nanoparticles are anionic.

Prior to the start of the thesis project, optimal layering ratios were determined for PLR and polyanions. In addition, it was determined that up to 2 mg Angiopep-2-Cys (AP2) per mg nanoparticle could be layered onto both HA and PLD nanoparticles without leading to nanoparticle charge conversion or aggregation. Preliminary *in vitro* experiments were conducted to probe the efficacy of electrostatically adsorbed AP2 on the transport of the nanoparticles in a transwell model of the BBB, but results were inconsistent and nanoparticles seemed to be unstable under physiological salt conditions. Originally, I planned to conduct molecular dynamics simulations to probe whether the segment of Angiopep-2 that targets the LRP1 receptor was buried into the polyanion layer; however, I found that manipulating the pH of the layering buffer for peptide adsorption led to consistent results both *in vitro* and *in vivo*. With this success, I continued with the original experimental plan, which included particle characterization, *in vitro* experiments in a transwell model of the BBB, and *in vivo* intravital imaging in mice.

Chapter 2: Materials and Methods

Several components of this section are similar to the corresponding section of Lamson et al.[1] I have reproduced the relevant sections below and supplemented them with methods specific to this work.

2.1. Materials

1,2-distearoyl-sn-glycero-3-phospho-(1'-rac-glycerol)   sodium   salt   (DSPG), 1,2-distearoyl-sn-glycero-3-   phosphoethanolamine   (DSPE),   1,2-distearoyl-sn-glycero-3-phosphoethanolamine-N-(Cyanine 5) (DSPE-Cy5), 1,2-distearoyl-sn-glycero-3-phosphocholine (DSPC) and cholesterol were purchased from Avanti. Chloroform was purchased from TCI. Methanol, the hCMEC/D3 cell line, Accumax dissociation reagent, Type 1 rat tail collagen, ascorbic acid, dimethyl sulfoxide (DMSO), Tris (2-carboxyethyl) phosphine (TCEP), 10X TBE Buffer (Tris-borate-EDTA), and heparin sulfate were purchased from MilliporeSigma. Whatman Nucleopore polycarbonate hydrophilic membranes (400, 200, 100 and 50 nm sizes) were purchased from GE. 50/15 mL Falcon tubes, Protein LoBind tubes, Polystyrene semi-micro cuvettes, microscope slides, coverslips, and slide sealer nail polish were purchased from VWR. D02-E300-05-ND, 02-E100-05-N, and C02-E100-05-N tangential flow filtration filters were purchased from Repligen. Poly-L-arginine hydrochloride (38.5 kDa) and poly-L-aspartic acid (15 kDa) were purchased from Alamanda Polymers. Hyaluronic acid (40 kDa) was purchased from LifeCore Biomedical. DTS 1070 folded capillary zeta cells were purchased from Malvern. Tissue culture plasticware (T75, T25, clear and white 96 well plates), 24-well 1 µm pore transwell plates, individual transwell inserts, Penicillin/Streptomycin and fetal bovine serum (FBS) were purchased from Corning. EBM-2 cell culture media was purchased from Lonza. Phosphate buffered saline (PBS), chemically defined lipid concentrate, 1 M bioreagent-grade

HEPES, and basic fibroblast growth factor were purchased from Thermo Fisher. ABD-F was purchased from Fisher Scientific. The Voltohmmeter and accompanying electrodes were purchased from World Precision Instruments. Peptides were synthesized by the Biopolymers & Proteomics core facility at the Swanson Biotechnology Center at the Koch Institute for Integrative Cancer Research at MIT.

2.2. Nanoparticle Synthesis and Characterization

2.2.1. Liposome Synthesis

Cholesterol and DSPC stocks were prepared at 25 mg/mL in chloroform, DSPG stocks were prepared at 25 mg/mL in 2:1 chloroform : methanol, and DSPE stocks were prepared at 5 mg/mL in 2:1 chloroform : methanol. Cholesterol and lipid stocks were then combined in a round bottom flask at a molar ratio of 31 Chol: 31 DSPC : 31 DSPG : 6.6 DSPE : 0.4 Cy5-DSPE. The lipids were dried into a thin film using a BUCHI RotoVap system under heat (55°C) and vacuum (30 mBar) for one hour. Milli-Q deionized water heated to 65°C was added to the round bottom flask to resuspend the lipid film to a 1 mg lipid/mL solution, thus forming liposomes. The solution was sonicated three times for [1 minute on, 1 minute off] at 65°C. Liposomes were extruded with an Avestin LiposoFast LF-50 liposome extruder, which was connected to a Cole-Parmer Polystat Heated Recirculator Bath held at 65°C. Liposomes were extruded twice through 400 nm, 200 nm, and 100 nm nucleopore membranes, and once through a 50 nm nucleopore membrane until the Z-average liposome size was less than 90 nm and the PDI was less than 0.200 (as determined by dynamic light scattering (DLS)).

2.2.2. Layer-by-Layer Polymer Functionalization

Polyelectrolyte solutions were prepared in 50 mM HEPES (pH 7.4) and 40 mM NaCl, with the exception of HA, which was prepared in 2 mM HEPES (as determined by Boehnke et al.).[28]

Weight equivalents (wt. eq.) of polyelectrolyte used with respect to liposome core were optimized through a test batch protocol, wherein the amount of polymer needed to fully charge convert the liposome was determined on the DLS by following the below procedure (minus purification) with 50 uL of liposome solution and 50 uL of polymer solution at a range of concentrations between 0 wt. eq. and 2 wt. eq. Liposomes were layered by adding liposome solution (0.5 mg/mL when layering HA, 1 mg/mL otherwise) to an equal volume of polyelectrolyte solution at the optimal concentration under sonication at room temperature. The mixture was sonicated for three seconds then vortexed for ten seconds. Layered particles were incubated at room temperature for 10 minutes, then purified using tangential flow filtration.

2.2.3. Layer-by-Layer Peptide Functionalization

Peptide solutions were prepared in a fresh (less than 8 hours old) solution of 0.6 mg/mL TCEP reducing agent in 20 mM HEPES (pH 7.4). TCEP is present as an agent to prevent disulfide bonds from forming between cysteine residues of adjacent peptides.[28] Cationic peptides were electrostatically layered onto negatively-charged layer-by-layer liposomes at layering ratios low enough to maintain the net anionic surface charge of the nanoparticles and preventing aggregation by keeping the zeta potential under -30 mV. Protein Lo-Bind tubes were used for all steps of the peptide layering process to minimize peptide loss. The maximum layering ratio for peptides was determined through a series of test batches similar to the outer layer test batches described above wherein 50 uL of nanoparticle solution (1 mg/mL with PLD-layered particles, 0.5 mg/mL with HA-layered particles) were combined 50 uL of peptide solution at a range of concentrations between 0 wt. eq. and 4 wt. eq. The maximum peptide layering ratio was determined by the maximum amount of peptide that was layered onto the nanoparticles without the zeta potential exceeding -30 mV.

2.2.4. Tangential Flow Filtration

Samples to be purified were connected to a Spectrum Labs KrosFlo II filtration system using Masterflex, Teflon coated tubing. D02-E100/E300-05-N filters were used for batch volumes < 12 mL and C02-E100-05-N filters were used for batch volumes > 12 mL. A 300 kDa molecular weight cutoff was used for HA purification and a 100 kDa molecular weight cutoff was used for all other purifications. For all purifications, the filter was pre-treated using a mock sample of free polymer (or peptide), to saturate adsorption sites on the membrane walls. Samples were filtered at 13 mL/min for small batches or 80 mL/min for large batches, with a Milli-Q water inlet line to replace 1:1 the volume of waste permeate. After at least 5 sample volume equivalents of waste collection, the sample was concentrated, removed from the filter by reversing the pump direction, and brought back to 1 mg/mL nanoparticle concentration for PLR and PLD nanoparticles, 0.5 mg/mL nanoparticle concentration for HA nanoparticles, and 0.4 mg/mL for peptide nanoparticles by backflushing a defined volume of Milli-Q water through the filter and into the sample.

2.2.5. TEM

Nanoparticle images were taken using a JEOL 2100 field emission gun (FEG) TEM. Samples were frozen in DI water and sent to the Koch Institute Nanotechnology Materials Facility. Specifically, 3 μL LbL NP sample in DI water was deposited on a copper grid coated with a continuous carbon film and blotted to remove excess sample without damaging the carbon layer by Gatan Cryo Plunge III. The grid was mounted on a Gatan 626 single tilt cryoholder equipped in the TEM column. The specimen and holder tip were cooled by liquid nitrogen. Imaging on the JEOL 2100 FEG microscope was done using the minimum dose method to avoid sample damage under the electron beam. The microscope was operated at 200 kV and with a magnification of

10,000 to ~60,000 for assessing particle size and distribution. All images were recorded on a Gatan 2kx2k UltraScan charge-coupled device camera.

2.2.6. Liposome Characterization

Nanoparticle hydrodynamic size, polydispersity, and zeta potential were measured using dynamic light scattering (Malvern ZS90 Particle Analyzer, λ= 633 nm). 50 µg of each nanoparticle was diluted into Milli-Q water (if nanoparticle sample was already in a salt solution) 2 mM NaCl (if nanoparticle sample was not in a salt solution) to give a total volume of 800 µL, then transferred to polystyrene cuvettes (size measurement) or DTS1070 folded capillary cuvettes (zeta potential measurement) for DLS.

2.2.7. Stewart Assay for Liposome Concentration Determination

Ammonium ferrothiocyanate solution (Stewart's reagent) was prepared by dissolving 27.03 g ferric chloride hexahydrate and 30.4 g ammonium thiocyanate in DI water and volumizing to 1 L. 0.060 mg of each liposome sample was brought up to 1 mL of volume with chloroform, then added to 1 mL of Stewart's reagent. 1 mg/mL solution of phospholipids and cholesterol at the ratio listed in section 2.1 was prepared in 2:1 chloroform : methanol; amounts ranging from 0 mg to 0.1 mg of the lipid solution were subjected to the steps above for the standard curve. Each tube was vortexed for 20 seconds, then centrifuged for 10 minutes at 1000 rpm (300 g). Samples were taken from the lower chloroform layer and plated in a polypropylene 96-well plate. The samples were then read for absorbance at 485 nm on a Tecan Infinite M200 Pro plate reader, and particle concentrations were determined relative to the standard curve.

2.2.8. Peptide Quantification Through Detection of Free Thiols with ABD-F

This protocol is modified from that given by Boehnke et al.[28] Nanoparticle concentrations were standardized via fluorescence. Nanoparticle samples were diluted 1:1 with 1x Tris-borate-EDTA buffer, pH 8.0, containing 2 mM TCEP. Standard curve samples prepared with Angiopep-2 were prepared in the same buffer. Sample solutions diluted 1:1 with 1x Tris-borate-EDTA buffer, pH 8.0, containing 1 mM ABD-F. Vials were heated for 5 minutes at 50°C in a sonicator bath, then cooled in an ice bath. 100 mM HCl aqueous solution was added to each vial to stop the reaction. Samples were transferred to a black 96-well plate, then read for fluorescence on a Tecan Infinite M200 Pro plate reader (excitation: 389 nm, emission: 513 nm). Peptide concentrations were calculated based on standard curve fluorescence readings.

2.3. Cell Culture

2.3.1. Maintenance

hCMEC/D3 cells were cultured according to manufacturer specifications in EBM-2 media supplemented with 5% FBS, 1 ng/mL bFGF, 1.4 μM hydrocortisone, 1% pen/strep, 1% chemically defined lipid concentrate, 10 mM HEPES, and 5 μg/mL ascorbic acid. Cells were cultured in flasks coated with 12 μg/cm2 rat tail collagen and split twice per week at a ratio between 1:4 and 1:6 using Accumax dissociation reagent, to maintain cells below approximately 90% confluency. Between maintenance and experiments, cells were incubated at 37 °C and in a 100% humidity and 5% CO2 atmosphere. Cells were tested monthly for mycoplasma, with all results coming back negative for contamination.

2.3.2. Cell Monolayers for Uptake Experiments

hCMEC/D3 cells were suspended in media and seeded at a density of 2×10^5 cells/cm^2 in collagen-coated (12 μg/cm^2) transwell supports. The cells were incubated for 6-8 days, with media replacement every 2-3 days. The TEER (expressed as resistance of transwell filters with

cells minus transwell filters without cells) was monitored to confirm proper barrier formation before use in any experiments.

2.4. Transport Experiments

2.4.1. General Protocol

Cell monolayers in transwells were transferred to 24-well plates containing 1 mL/well media. Nanoparticles were added to the apical chambers at 20 µg/cm^2 in media; negative control wells received fresh media. Extra treatments for each experiment were used to make fluorescence calibration curves. At 4, 8, and 24 hours after treatment addition, the monolayers were transferred to new basal plates. Media from the basal plates was sampled for fluorescence measurements on a Tecan Infinite M200 Pro plate reader, with 100 µL/well sample in a black 96-well plate, and applied to the calibration curves to calculate percent of nanomaterial transported.

2.4.2. DMSO Breakup and Reread for Liposomes

To homogenize fluorescent liposome containing samples, 100 µL of sample (nanoparticles in cell culture media) per well was supplemented with 100 µL/well DMSO and 50 µL/well of heparin sulfate (1 mg/mL in PBS). The plate was placed on an orbital shaker at 300 RPM for 15 minutes before repeating the fluorescence measurements.

2.5. Animal Studies

2.5.1. Animal Care and Use

All animal experiments were approved by the Massachusetts Institute of Technology Committee on Animal Care (CAC, protocol number 0919-056-22) and were conducted under the oversight of the Division of Comparative Medicine (DCM). C57BL/6 mice were purchased from Taconic, and were housed in cages of no more than five animals with controlled temperature (25 °C), 12 h

light−dark cycles and free access to food and water. Both female and male mice were used in this study, and the mice were 35-40 weeks old at the time of experiment. leading to one group 3 female mice and one group of 2 female + 1 male mice, with 1-3 measurements per animal.

2.5.2. Intravital Imaging

Mice underwent head hair removal up to 24 hours before the imaging procedure occurred. One at a time, animals were injected with 70 kDa FITC-labeled dextran (2 mg/mL in PBS, sterile filtered) and red fluorescent nanoparticles (1 mg/mL in 5% dextrose), both as 150 μL retro-orbital injections. To create the cranial window, the skull was exposed, and a high-speed hand drill (Dremel) was used to thin the skull until the dura mater was exposed over the right frontal cortex. The mice were then secured to a microscope coverslip for imaging. Multiphoton imaging was performed on an Olympus FV-1000MPE multiphoton microscope (Olympus) using a 25×, numerical aperture 1.05 objective. Excitation was achieved by using a femtosecond pulse laser at 840 nm, and emitted fluorescence was collected by photomultiplier tubes with emission filters of 425/30 nm for Collagen 1, 525/45 nm for fluorescein isothiocyanate-labeled dextran, 607/45 nm for red polystyrene nanoparticles, and 672/30 nm for Cy5 (PLGA and liposome) nanoparticles. Collagen 1 was excited by second harmonic generation and emitted as polarized light at half the excitation wavelength. The collagen 1 signal was used to identify the dura, such that the vessels imaged were within the cortex. 19 Images were acquired every 2 minutes for 12 minutes for analysis, and up to three image sessions per mouse were run. Mice were maintained under anesthesia for the duration of the imaging and then humanely euthanized. Acquired images from intravital imaging were then thresholded and segmented by using the Fiji distribution of ImageJ and the Trainable Weka Segmentation plugin. Vessels below the dura and arteries were examined to ensure that these represent BBB capillaries in the mouse brain. The

microvasculature filled with dextran (dextran channel) was used to generate a three-dimensional mask of the BBB mouse vessels. This mask was employed to calculate vessel surface area, as well as dextran and nanoparticle signal both inside and outside the blood vessels. After masking, analysis of nanoparticle or dextran transport was performed as previously described.

Chapter 3: Nanoparticle Characterization

All nanoparticles tested consisted of an anionic liposome, a cationic poly-L-arginine (PLR) second layer (0.4 mg PLR per mg liposome core), and an anionic outer layer (either poly-L-aspartate (PLD), with a layering ratio of 0.8 mg PLD per mg liposome core, or hyaluronate (HA), with a layering ratio of 1.2 mg HA per mg liposome core). These optimal layering ratios were determined prior to this work, and Stewart assays were performed at each step to determine nanoparticle concentration so that layering ratios were accurate. All peptides chosen were cationic, linear peptides. Peptides were layered onto PLR-PLD and PLR-HA liposomes without fully covering the surface of the nanoparticle such that the overall surface charge remained negatively charged. A schematic of the LbL assembly is shown in **Figure 1**.
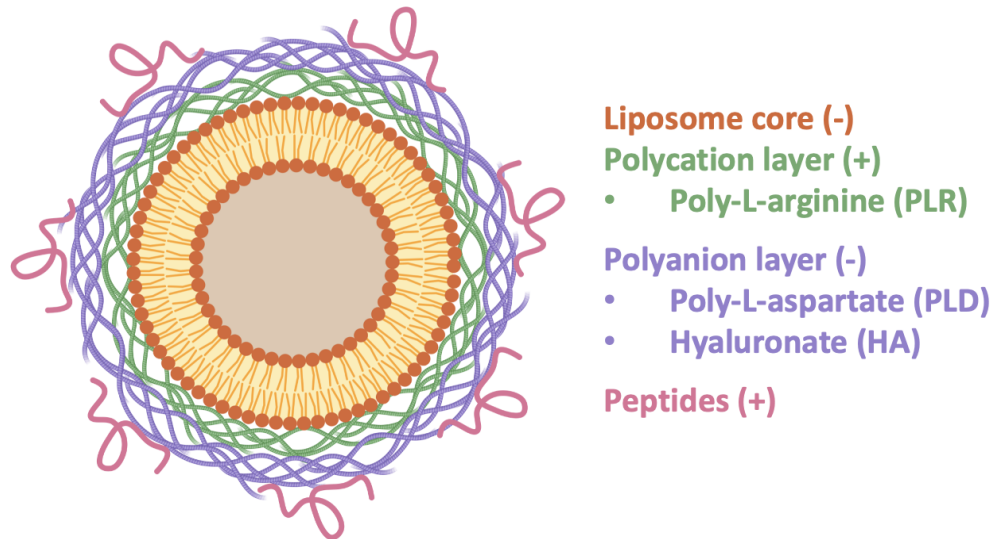
Liposome core (-)
Polycation layer (+)
• **Poly-L-arginine (PLR)**

Polyanion layer (-)
• **Poly-L-aspartate (PLD)**
• **Hyaluronate (HA)**

Peptides (+)

Figure 1: Schematic of LbL liposomal nanoparticle. Electrostatic layer-by-layer adsorption of cationic peptides allows for functionalization of the surface of liposomal nanoparticles.

A series of linear cationic peptides (with sequences, charges, and masses shown in **Table 1)** were obtained from the Koch Institute's Biopolymers and Proteomics core. Cyclic peptides were excluded from this study due to Boehnke et. al.'s findings that cyclic peptides were less effective at forming polyion complexes and completely covering the surface of the nanoparticle than linear peptides.[28] Peptides were selected to have a mass between 1.0 and 3.5 kDa and a charge between +1 and +4 at physiological pH (7.4) to enable electrostatic attraction between peptides and anionic layers without fully charge converting the nanoparticle. Cysteine residues were added to peptides that did not already contain them (Angiopep-2, RAP12, and Substance P) for easy peptide quantification via a thiol-based detection assay. Cysteine placement at the C-terminus was shown to not affect BBB-penetrance of Angiopep-2 and RAP12, and addition of a thiol group to the N-terminus of Substance P also did not affect BBB-penetrance.[13,29,30]

Peptide Name	Sequence	Mass (kDa)	Charge at pH 7.4
Angiopep-2-Cys (AP2-Cys)	TFFYGGSRGKRNNFKTEEYC	2.4	+2
RAP12-Cys	EAKIEKHNHYQKC	1.6	+1.1
RVG29	YTIWMPENPRPGTPCDIFTNSRGKRASNG	3.3	+2
G23	HLNILSTLWKYRC	1.6	+2
Peptide drug G - anti G (pGaG)	CGNKRTRGGGLFDIIKKIAESF	2.4	+3
Cys-Substance P (Cys-SubP)	CRPKPQQFFGLM	1.4	+2
B6	CGHKAKGPRK	1.0	+4

Table 1: Characteristics of peptides used in this study. To determine charge at pH 7.4, amino acids D (aspartate) and E (glutamate) were assigned -1 charge, and amino acids K (lysine) and R (arginine) were assigned +1 charge. As per Tu et al., H (histidine) was assigned +0.05 charge.[31]

Test batches were conducted to determine how layering cationic peptides at different ratios onto nanoparticles with PLD and HA outer layers affects nanoparticle size and zeta potential (interpreted as an analog to nanoparticle surface charge). As per Correa et al., we consider nanoparticles with Z-average size less than 200nm and absolute zeta potential greater than 30 mV to be colloidally stable; however, HA particles have demonstrated stability with measured zeta potential as high as -25 mV.[24] DLS measurements (Z-average size and zeta potential) were recorded both before and after peptide adsorption under the same salt conditions (10 mM HEPES + 0.3 mg/mL TCEP). The results are shown in **Figure 2.**
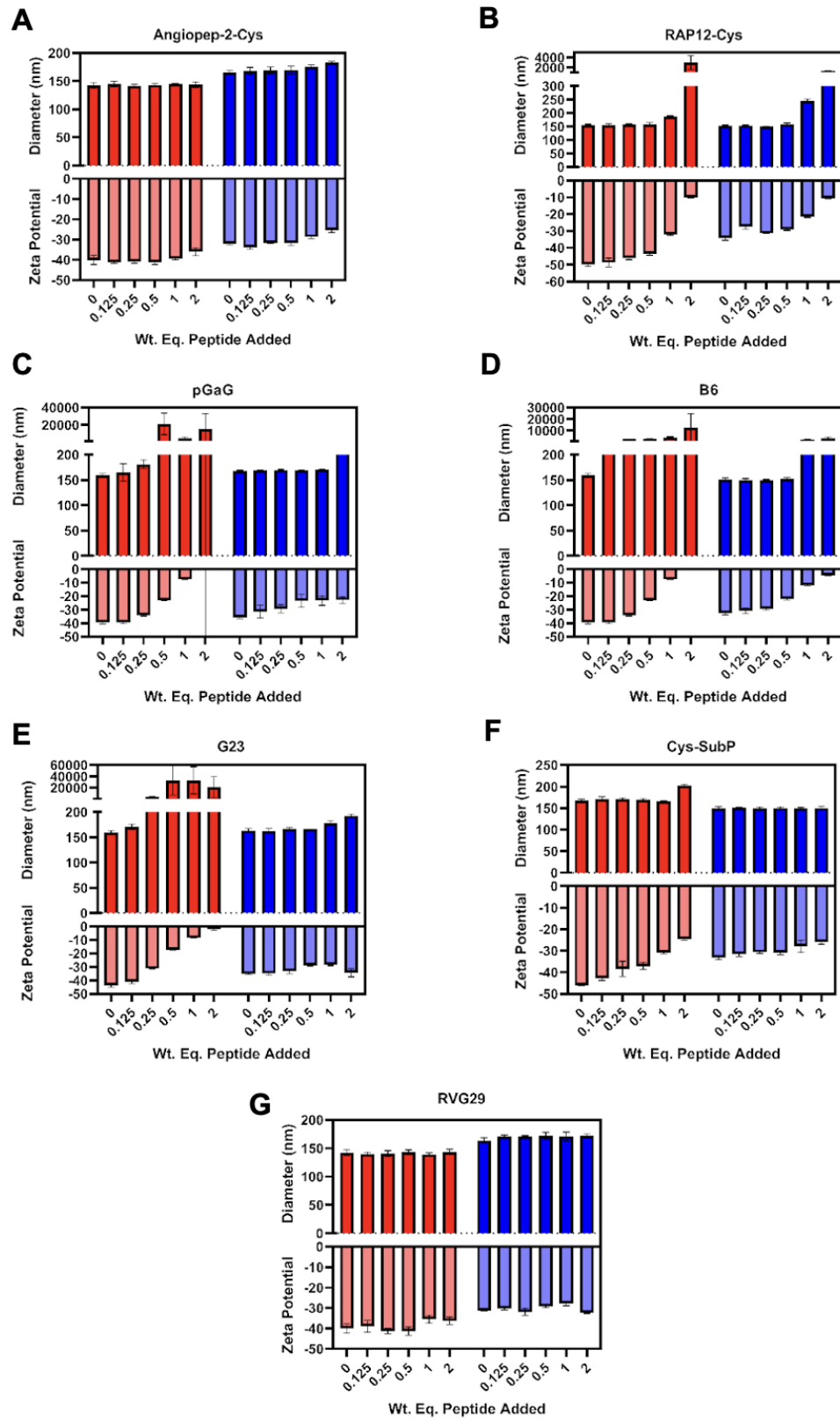
Figure 2: Optimal layering ratio of cationic peptides onto anionic LbL nanoparticles depends on peptide charge-to-mass ratio and anionic outer layer chemistry. The seven different peptides included in test batches are shown in Figures 2A-G.

Adsorption of small peptides with highly concentrated charge (B6, pGaG, Cys-SubP, and G23) led to aggregation of PLD nanoparticles at fairly low layering ratios (0.25 wt. eq. or lower), while HA nanoparticles functionalized with these peptides were stable up to much higher layering ratios (0.5 wt. eq. for B6, the peptide with the highest charge-to-mass ratio (**Figure 2D**), 1 wt. eq. for Cys-SubP and pGaG (**Figures 2F** and **2C**, respectively), and 2 wt. eq. for G23 (**Figure 2E**)). This difference could be due to the high capacity of HA for cationic charge shielding due to its loose chain packing and high chain interspersion. I hypothesized that HA chains would prevent small cationic peptides from accessing the surface of the nanoparticle, which may prevent improvement in BBB transport efficiency from peptide-functionalized HA nanoparticles. AP2- and RVG29-functionalized nanoparticles were stable on both PLD and HA nanoparticles at all peptide layering ratios tested (**Figures 2A** and **2G**, respectively), and nanoparticles functionalized with RAP12-Cys (the tested peptide with lowest charge at physiological pH and an intermediate charge-to-mass ratio) were stable up to 0.5 wt. eq. of peptide added (**Figure 2B**).

Based on these test batches, AP2-Cys was chosen for further testing, since it layered stably onto both PLD and HA particles in the entire range of layering ratios, and its BBB-penetrance and lack of cytotoxicity are well characterized in the literature; AP2-linked drugs are currently in clinical trials.[32] In addition, the interactions between RAP12-Cys and LbL nanoparticles were further characterized, since particles functionalized with 1 wt. eq. RAP12-Cys aggregated despite RAP12-Cys having a relatively low charge-to-mass ratio at physiological pH.

Batches of AP2-Cys-functionalized (0.2 wt. eq. and 2 wt. eq.) PLD and HA particles were synthesized and purified, and an ABD-F-based free thiol detection assay was conducted to

quantify the amount of peptide that remained post-purification (**Figure 3AB**). Since greater than 80% of the peptide remained on the nanoparticle post-purification for both outer layers, I concluded that AP2-Cys layering is highly efficient even at high weight equivalents. I also performed peptide quantification on RAP12-Cys-functionalized PLD and HA particles at 0.5 wt. eq. (the highest layering ratio at which the particles were stable in test batches) synthesized in layering buffers titrated to pH 5.5 (close to the pKa of histidine, meaning that RAP12-Cys should carry +2 charge) and pH 7.4 (physiological pH, where RAP12-Cys carries approximately +1.1 charge). (**Figure 3C**). I originally hypothesized that layering efficiency would decrease with increasing pH due to weaker charge interactions between the peptides and the anionic outer layers, but this effect was not observed (although experiments to confirm and investigate this behavior are ongoing).

In order to evaluate the effect of peptide adsorption on the colloidal stability of LbL nanoparticles in salt solutions, PLD, PLD-AP2-Cys (2 wt. eq. peptide), HA, and HA-AP2-Cys (2 wt. eq. peptide), were incubated in NaCl solutions ranging from 7.8 mM to 1.0 M for eight hours. Nanoparticle size was measured at the end of the interval through DLS (Figure 4). Adsorbing AP2-Cys to PLD-coated nanoparticles limits the ability of the nanoparticle to withstand high salt concentrations: PLD particles were stable up to 125 mM NaCl, whereas PLD-AP2-Cys nanoparticles were only stable up to 31.3 mM NaCl. Because PLD-AP2-Cys-coated nanoparticles I' have a less negative zeta potential than PLD-coated nanoparticles, lending less electrostatic colloidal stability, they are more likely to aggregate when exposed to salt conditions. HA-coated nanoparticles were less resistant to high salt concentrations and were only stable up to 15.6 mM NaCl; however, adsorbing AP2-Cys did not further limit stability in salt solution. This further supports the previous hypothesis that HA

chains prevent AP2-Cys from accessing the surface through a charge screening mechanism, as stability in salt solutions is highly dependent on surface properties of the nanoparticle.
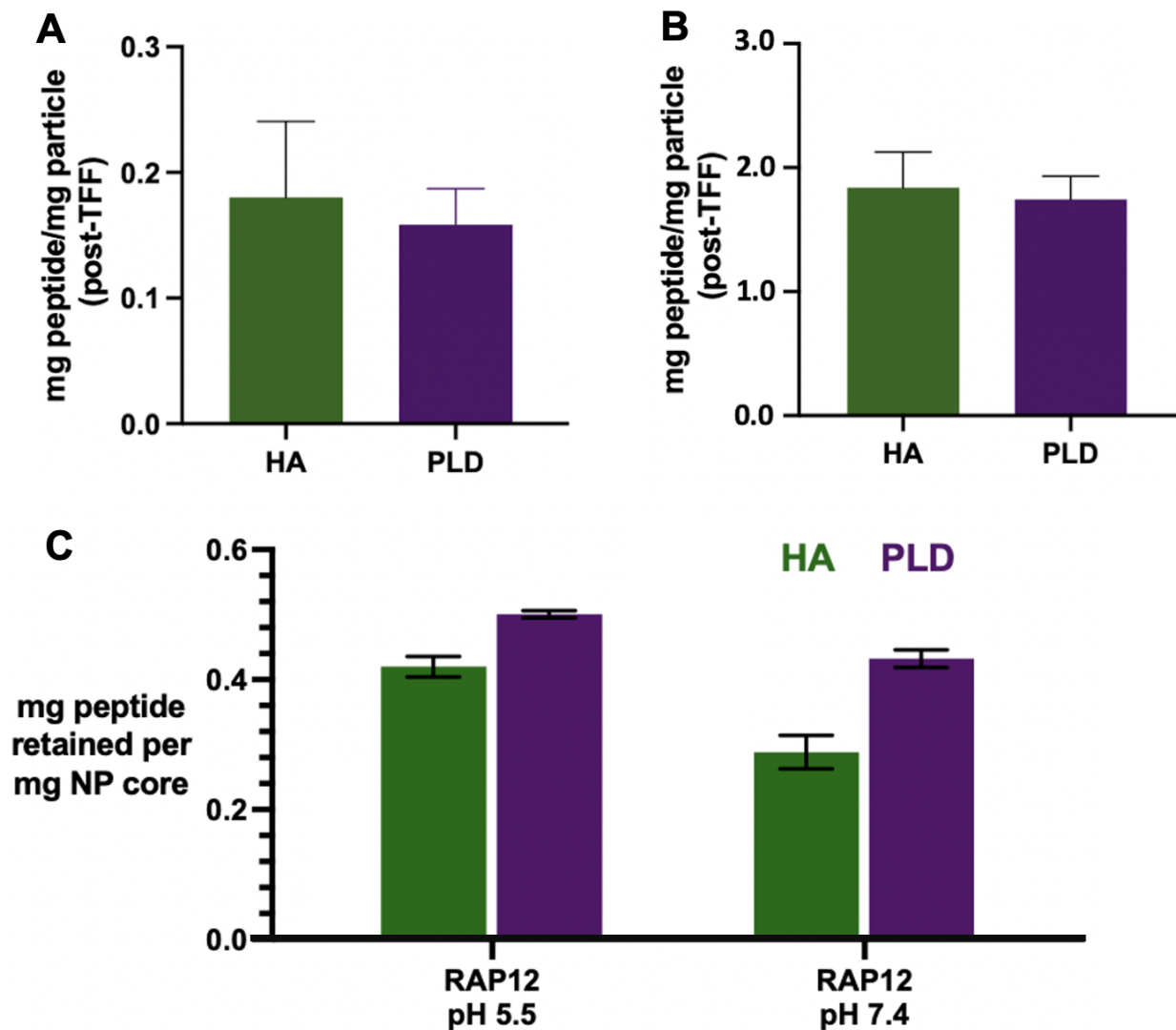

Figure 3: Results of ABD-F free thiol detection assay on AP2-Cys- and RAP12-Cys-functionalized particles.
Figure 3AB: retention of Angiopep-2-Cys (0.2 wt. eq. and 2 wt. eq. layered) on PLD- and HA-layered nanoparticles.
Figure 3C: retention of RAP12-Cys (0.5 wt. eq.) on PLD- and HA-layered nanoparticles.

While physiological NaCl concentration in serum (150 mM) is higher than the NaCl concentration at which the nanoparticles are stable, it is hypothesized that peptides and proteins present in serum can provide additional colloidal stability to nanoparticles.[28] To test this, the four nanoparticle samples subjected to the salt screen were incubated in hCMEC/D3 media (EBM-2

media supplemented with 5% FBS, 1 ng/mL bFGF, 1.4 μM hydrocortisone, 1% pen/strep, 1% chemically defined lipid concentrate, 10 mM HEPES, and 5 μg/mL ascorbic acid) for eight hours, then measured for Z-average size on the DLS. None of the four samples exhibited aggregation (zeta potential remained below -30 mV and Z-average diameter remained under 200 nm), indicating that the nanoparticles would be stable in physiological salt conditions.
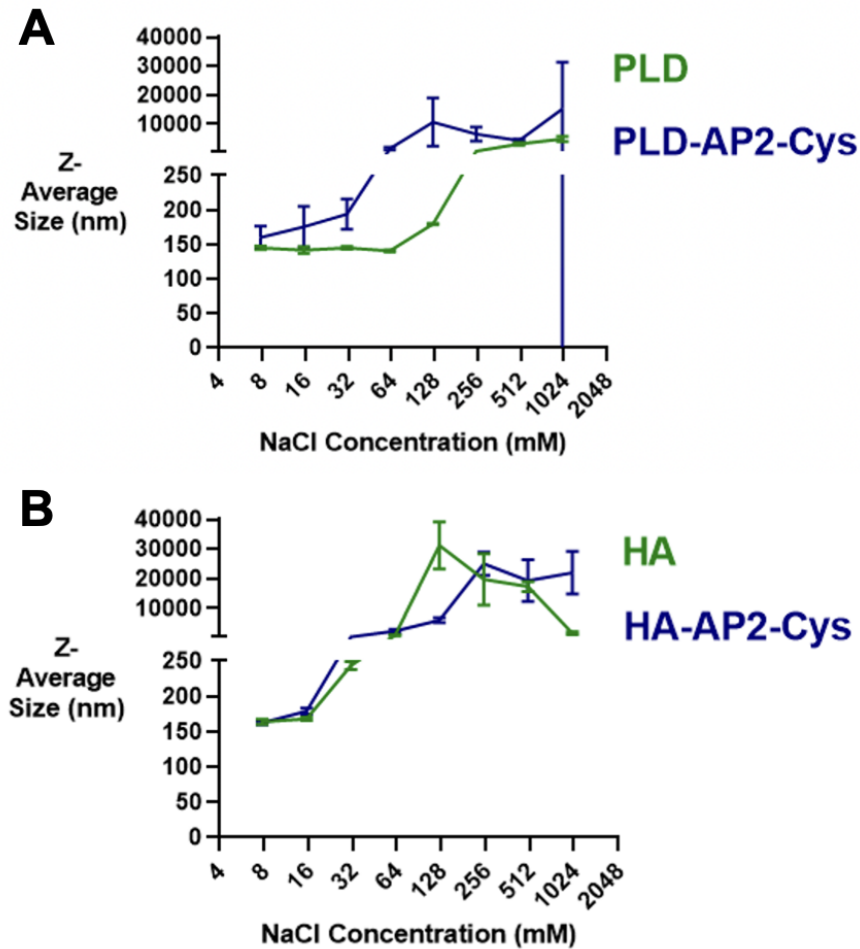

Figure 4: Results of salt screen (incubation of nanoparticle samples in NaCl solutions ranging from 7 mM to 1000 mM) for eight hours for AP2-functionalized and unfunctionalized PLD and HA particles. Figure 4A: PLD-coated nanoparticles demonstrate stability in stronger salt solutions than PLD-AP2-Cys-coated nanoparticles. 4B: HA-coated and HA-AP2-Cys-coated nanoparticles demonstrate stability in similar salt conditions.

As a final confirmation that the LbL nanoparticles used in this study retained their properties throughout the layering process, Cryo-TEM was performed to compare PLD-coated nanoparticles with PLD-Ap2-Cys-coated nanoparticles. Representative images are shown in **Figure 5.** There are no noticeable conformation differences between AP2-Cys-functionalized nanoparticles and unfunctionalized nanoparticles, as expected. Further analysis with ImageJ will be performed in order to quantify any differences in size distribution.
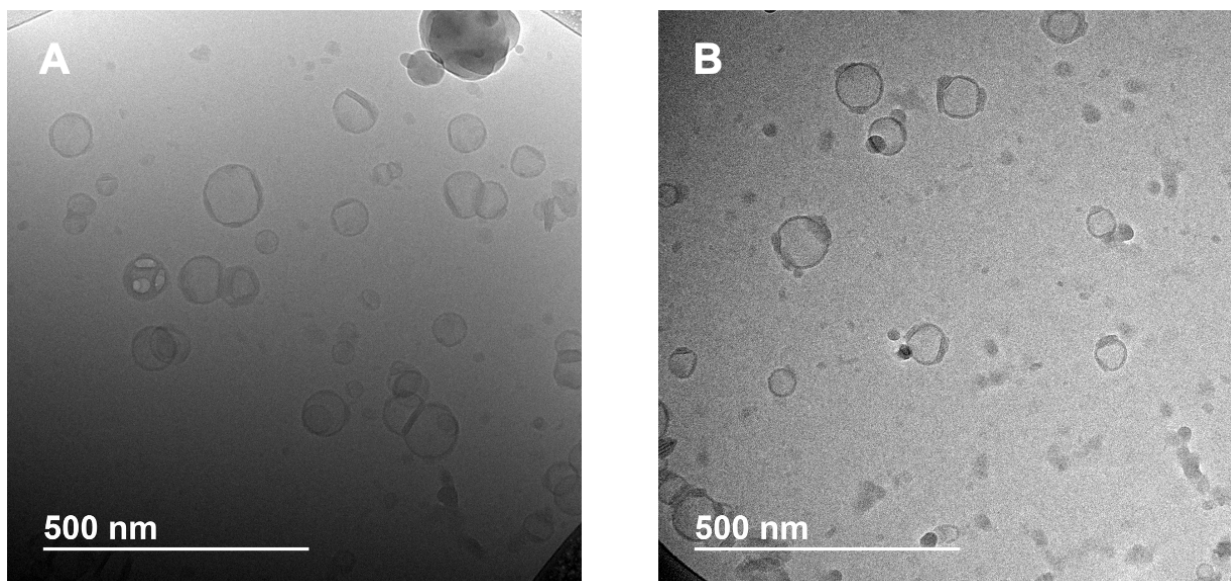
Figure 5: Representative cryo-TEM images of PLD (5A) and PLD-AP2-Cys (5B) nanoparticles. No clear differences between nanoparticle samples were observed through visual inspection, although further quantitative analysis is needed to determine any differences in nanoparticles size distributions.

Chapter 4: Screening of Nanoparticles in Cell Culture and Mouse Models of the BBB

Due to their endothelial phenotype and classic BBB protein expression (including the LRP1 receptor, which is the receptor for AP2), human-derived hCMEC/D3 immortalized microcapillary endothelial cells were chosen for *in vitro* experiments. To probe the efficacy of electrostatically adsorbed BBB-penetrating peptides in improving the BBB transport of LbL nanoparticles, a transwell model of the BBB was used (depicted in **Figure 6**). To ensure a balance between allowing for diffusion of 100 nm-200 nm nanomaterials through the membrane while avoiding significant media leakage over the course of the experiment, 1 um pore polyester transwell filters were chosen.
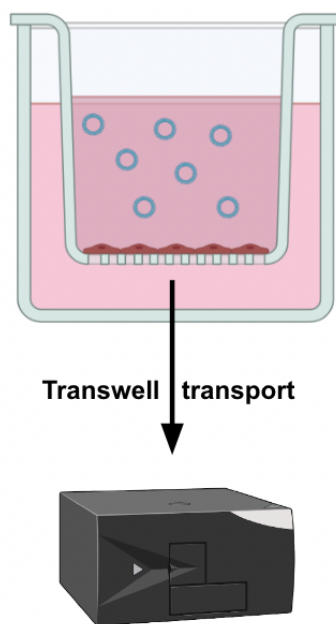

Figure 6: Transwell-supported membranes allow for growth of BBB-mimicking monolayers of hCMEC/D3 cells and subsequent evaluation of the ability of fluorescent nanoparticles to penetrate the cell monolayer.

PLD- and HA-coated particles were each functionalized with 2 wt. eq. of AP2-Cys as described in the previous section. In addition, to ensure that any improvement in transport was

due to receptor recognition of AP2-Cys and not modification of surface charge due to the adsorption of cationic peptides, a randomly generated scramble peptide of AP2-Cys (Scram-AP2-Cys) was synthesized (amino acid sequence: GRYRNTYGFKSTFFENGEKC). PLD-Scram-AP2-Cys and HA-Scram-AP2-Cys particles were also synthesized, each with two wt. eq. of peptide adsorbed to the nanoparticles. As shown in **Figure 7A**, PLD-coated nanoparticles functionalized with AP2-Cys appear to exhibit higher transport across the transwell-supported hCMEC/D3 monolayers than unfunctionalized PLD-coated nanoparticles and Scram-AP2-Cys functionalized nanoparticles, although due to biological variance between experiments (including variation between six and eight days of cell growth time before transwells were seeded with particles and variation of passage number of the cells at the time of the experiment).

To further investigate the effect of AP2-Cys while controlling for biological variance, a delta transport value for PLD-coated, PLD-AP2-Cys-coated, and PLD-Scram-AP2-Cys-coated nanoparticles was calculated for each plate by subtracting the average transport of the given sample from the average transport of PLD-coated nanoparticles on that plate. Thus, the delta transport value for a given nanoparticle sample on a given transwell plate. is equivalent to the improvement in transport demonstrated by that sample as compared to PLD-coated nanoparticles on the same transwell plate. These delta transport values were tabulated for all transwell experiments performed and compiled in **Figure 7B**. While differences between PLD, PLD-AP2-Cys, and PLD-Scram-AP2-Cys nanoparticles are nonsignificant at the 4 hour and 8 hour time points due to high variability, at 24 hours, the PLD-AP2-Cys nanoparticles demonstrate a significant transport advantage ($p < 0.05$) over both the PLD and PLD-Scram-AP2-Cys nanoparticles.
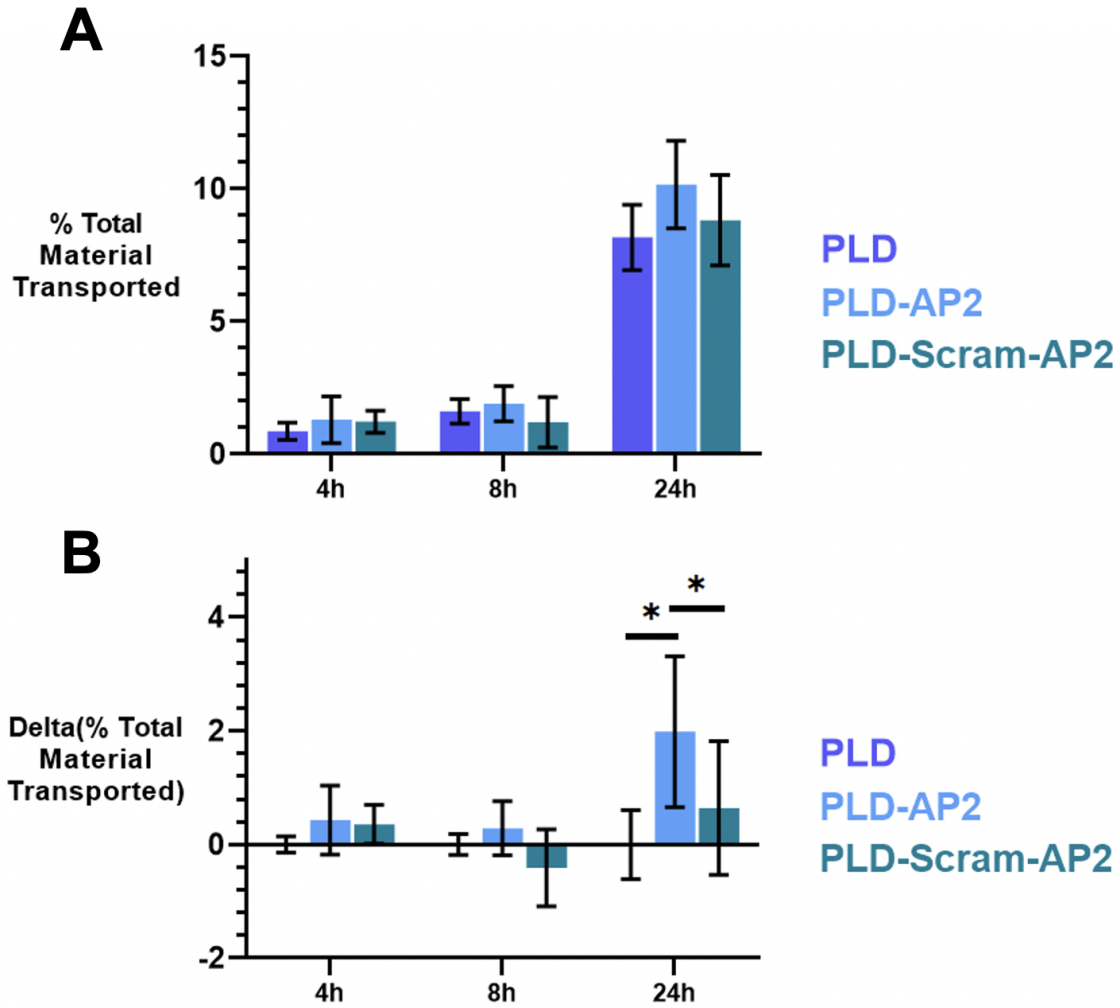
Figure 7: *In vitro* **transport experiments including PLD-coated nanoparticles demonstrate AP2-Cys-mediated improvement in BBB penetration.** 7A: Transcellular transport was measured in 3 biologically distinct transwell plates, and results did not indicate statistically significant improvement in transport from addition of AP2-Cys. 7B: Delta (% transport) was calculated by subtracting percent transport from the mean percent of PLD-coated particles transported within each biological replicate; here, a statistically significant improvement resulting from addition of AP2-Cys can be seen (as determined by a one-tailed t-test for samples with unequal variances).
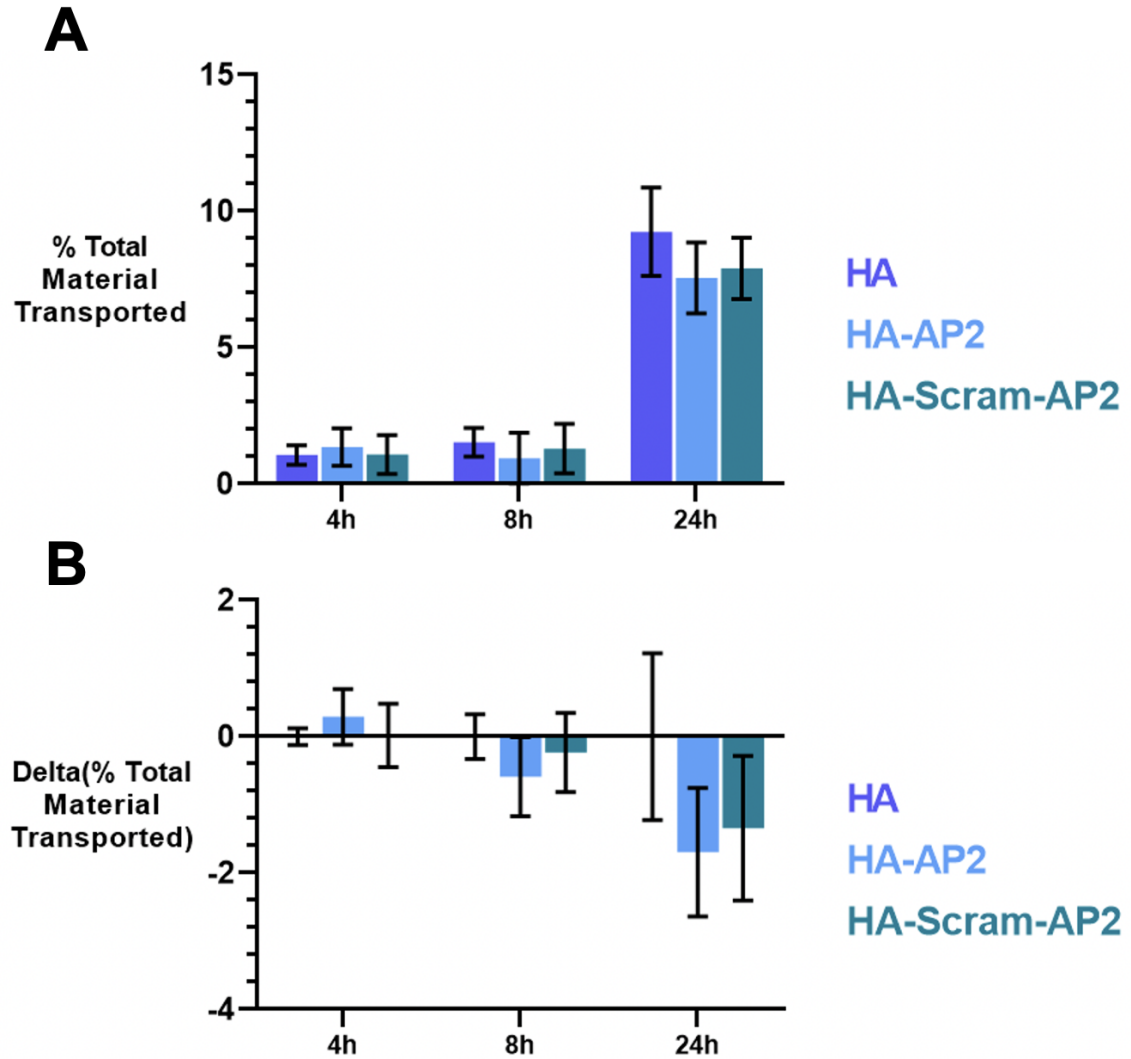
A

B

Figure 8: *In vitro* transport experiments including HA-coated nanoparticles do not demonstrate AP2-Cys-mediated improvement in BBB penetration. 8A: Transcellular transport was measured in 3 biologically distinct transwell plates, and results did not indicate statistically significant improvement in transport from addition of AP2-Cys. 8B: Delta (% transport) was calculated by subtracting percent transport from the mean percent of PLD-coated particles transported within each biological replicate; no improvement was observed from addition of AP2-Cys.

In contrast to PLD-coated nanoparticles, HA-coated nanoparticles do not demonstrate improvement in *in vitro* transport experiments when functionalized with either AP2-Cys or Scram-AP2-Cys (**Figure 8A**). When delta transport values were calculated, there remains no improvement in transport from peptide-functionalized particles (**Figure 8B**). This development

further supports the hypothesis that HA shields cationic peptides from the nanoparticle surface, thus severely limiting the bioactivity of the peptides.

The effect of nanoparticle size on efficacy of peptide-enhanced transport was also probed. Three different sizes of liposomes were synthesized; the first set (Lipo200) was extruded twice through 400 nm and 200 nm filters (Z-average diameter of 130.6 nm), the second set (Lipo100) was extruded twice through 400 nm, 200 nm, and 100 nm filters (Z-average diameter of 113.8 nm), and the third set (Lipo50) was extruded twice through 400 nm, 200 nm, and 100 nm filters and once through a 50 nm filter (Z-average diameter of 84.3 nm). Lipo50 is the set of liposomes used for all other components of this study. Each set was subjected to the same layering conditions: PLR, then PLD. Some of each sample was then functionalized with 2 wt. eq. of AP2-Cys. The results of screening all six formulations through a single bioreplicate of the transwell assay are shown in **Figure 9**.
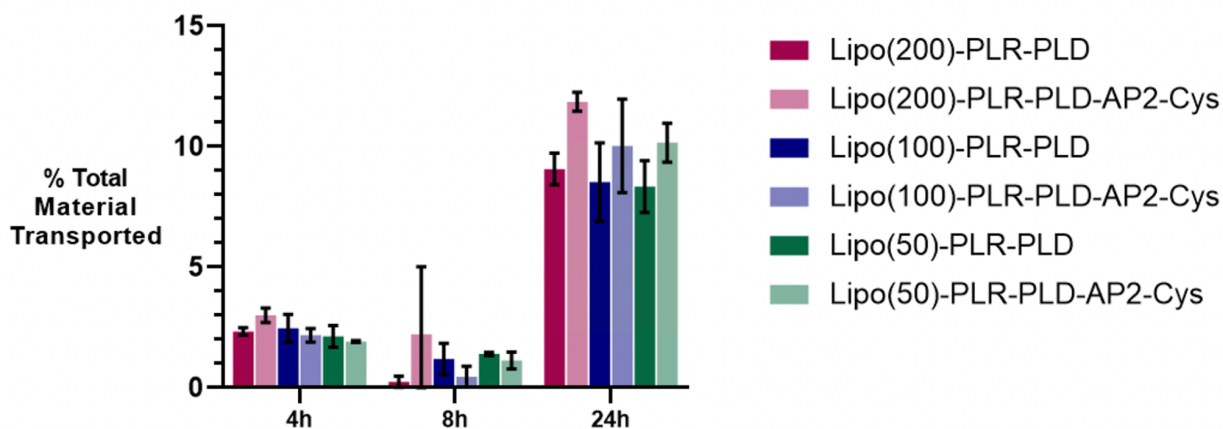

Figure 9: Modulating particle size between 85 nm (Lipo(50)) and 130 nm (Lipo(200)) does not appear to change the effect of electrostatically-adsorbed BBB-penetrating peptides on BBB permeability of the nanoparticles. Nanoparticles depicted here were synthesized from the same lipid and polymer aliquots and the same batch of AP2-Cys.

No significant differences in peptide-mediated improvement were found between the nanoparticle samples of different sizes. Thus, it is likely that electrostatically adsorbing peptides onto LbL systems with a variety of core diameters is possible, which is promising for future systems which might involve chemotherapy loading or different cores such as lipid nanoparticles (LNPs).

Since AP2-Cys-functionalized PLD-coated particles demonstrated improved *in vitro* BBB penetrance, I aimed to determine whether this effect was retained *in vivo*. To this end, nanoparticles were examined for BBB permeability with intravital imaging through a cranial window in mice as discussed by Lamson et al.[1] Fluorescent dextran signal from the first two-photon microscopy imaging time point is used to generate a mask to differentiate blood vessels from brain parenchyma. The remaining images in the series are compared, using the ImageJ software, to the mask in order to determine the permeability of the nanoparticles, relative to that of the dextran, across the BBB (**Figure 10A**). As observed in *in vitro* transwell experiments, PLD-coated particles functionalized with AP2-Cys (2 wt. eq.) exhibited higher BBB permeability *in vivo* than un-functionalized PLD-coated particles (**Figure 10B**). Due to time and resource limitations, the study only featured six mice (three for each treatment group), so it was not possible to screen PLD-coated particles functionalized with Scram-AP2-Cys or to determine statistical significance.
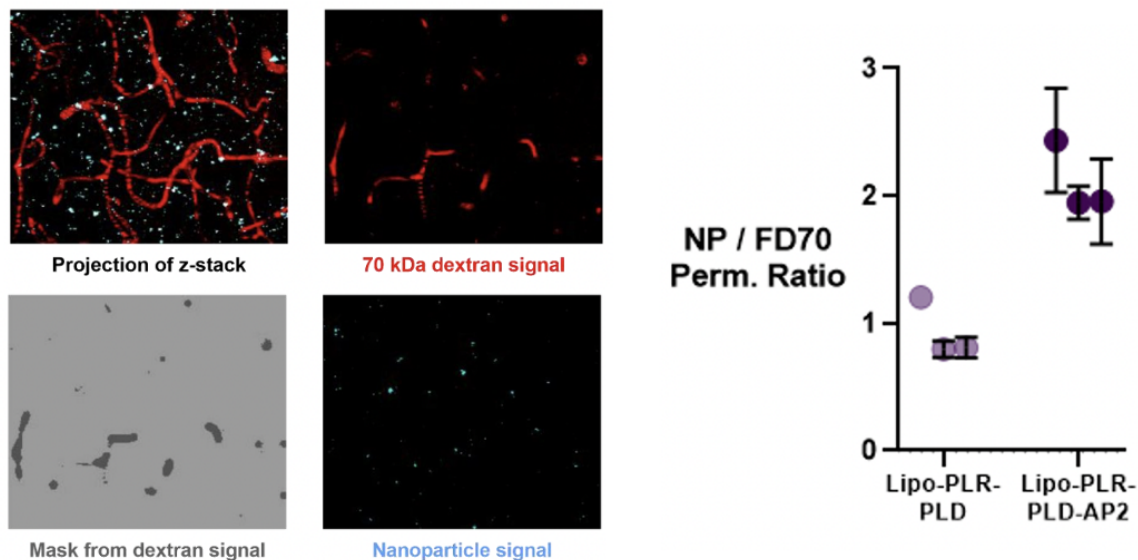
Figure 8: Intravital imaging allows for comparison of nanoparticle permeability across a mouse model of the blood brain barrier. From a series of z-stack images, a mask of 70 kDa FITC-dextran is created to visualize the placement of blood vessels in the brain. Nanoparticle signal outside of this mask is then quantified and used as a measure of nanoparticle permeability. Only three mice were used for each treatment group, so statistics were not applied to calculate significance of the improvement in permeability resulting from adsorption of AP2-Cys.

Chapter 5: Conclusions and Future Work

This work demonstrates that electrostatic adsorption of cationic BBB-penetrating peptides to the surface of anionic LbL nanoparticles is an effective strategy for improving BBB transport of nanocarriers. Nanoparticles functionalized with Angiopep-2-Cys are adequately stable under physiological salt conditions, and demonstrate improved transport across an *in vitro* model of the BBB. In addition, within the 85 nm-130 nm Z-average diameter range, nanoparticle core size was shown to not affect the improvement derived from BBB-penetrating peptides, so this approach can be extended to larger nanoparticle cores if necessary for a particular application. In preliminary intravital imaging studies in mice, peptide-functionalized

nanoparticles also demonstrate improved BBB penetrance when compared to unfunctionalized nanoparticles.

Ongoing work includes repeating the intravital imaging experiments with HA- and HA-AP2-Cys-coated nanoparticles and repeating the intravital imaging experiment with PLD-coated nanoparticles with the addition of PLD-Scram-AP2-Cys nanoparticles and more mice so conclusions about statistical significance can be drawn.

In the future, to compare the effectiveness of electrostatic adsorption of peptides with other chemistry-based strategies on the LbL nanoparticle platform, I will conjugate maleimide groups to the ends of the chains of the outermost polymer layer, then functionalize them with AP2-Cys through a Cys-maleimide bioconjugation reaction. I will then use this functionalized polymer as the final layer of the LbL nanoparticle, and compare its transport with the electrostatically functionalized nanoparticles. Experiments will also be repeated with liposomes loaded with common brain-targeted chemotherapies, such as doxorubicin or erlotinib, to ensure that this proposed method for nanoparticle functionalization does not break down once drugs are loaded into the liposome.

Future bioassays will include a cytotoxicity assay (although both AP2-Cys and LbL nanoparticles have been demonstrated to be non-cytotoxic, so we do not expect to see toxicity) and a biodistribution assay. In addition, uptake into glioma cells (rather than healthy hCMEC/D3 cells) will be assessed to determine whether glioma cell phenotype affects the impact of AP2-Cys. Finally, *in vivo* intravital imaging experiments will be repeated in immunocompromised mice.

Acknowledgements

References

(1) Lamson, N. G.; Pickering, A. J.; Wyckoff, J.; Ganesh, P.; Straehla, J. P.; Hammond, P. T. *Core Material and Surface Chemistry of Layer-by-Layer (LbL) Nanoparticles Independently Direct Uptake, Transport, and Trafficking in Preclinical Blood-Brain Barrier (BBB) Models*; preprint; Bioengineering, 2022. https://doi.org/10.1101/2022.10.31.514595.

(2) Rock, K.; Mcardle, O.; Forde, P.; Dunne, M.; Fitzpatrick, D.; O'Neill, B.; Faul, C. A Clinical Review of Treatment Outcomes in Glioblastoma Multiforme—the Validation in a Non-Trial Population of the Results of a Randomised Phase III Clinical Trial: Has a More Radical Approach Improved Survival? *Br. J. Radiol.* **2012**, *85* (1017), e729–e733. https://doi.org/10.1259/bjr/83796755.

(3) Thakkar, J. P.; Dolecek, T. A.; Horbinski, C.; Ostrom, Q. T.; Lightner, D. D.; Barnholtz-Sloan, J. S.; Villano, J. L. Epidemiologic and Molecular Prognostic Review of Glioblastoma. *Cancer Epidemiol. Biomarkers Prev.* **2014**, *23* (10), 1985–1996. https://doi.org/10.1158/1055-9965.EPI-14-0275.

(4) Haumann, R.; Videira, J. C.; Kaspers, G. J. L.; Van Vuurden, D. G.; Hulleman, E. Overview of Current Drug Delivery Methods Across the Blood–Brain Barrier for the Treatment of Primary Brain Tumors. *CNS Drugs* **2020**, *34* (11), 1121–1131. https://doi.org/10.1007/s40263-020-00766-w.

(5) Lundy, D. J.; Lee, K.-J.; Peng, I.-C.; Hsu, C.-H.; Lin, J.-H.; Chen, K.-H.; Tien, Y.-W.; Hsieh, P. C. H. Inducing a Transient Increase in Blood–Brain Barrier Permeability for Improved Liposomal Drug Therapy of Glioblastoma Multiforme. *ACS Nano* **2019**, *13* (1), 97–113. https://doi.org/10.1021/acsnano.8b03785.

(6) Mondal, J.; Patra, M.; Panigrahi, A. K.; Khuda-Bukhsh, A. R. Improved Drug Carriage and Protective Potential against Cisplatin-Induced Toxicity Using Boldine-Loaded PLGA Nanoparticles. *J. Ayurveda Integr. Med.* **2020**, *11* (1), 24–36. https://doi.org/10.1016/j.jaim.2017.11.002.

(7) Gao, S.; Tian, H.; Xing, Z.; Zhang, D.; Guo, Y.; Guo, Z.; Zhu, X.; Chen, X. A Non-Viral Suicide Gene Delivery System Traversing the Blood Brain Barrier for Non-Invasive Glioma Targeting

Treatment. *J. Control. Release Off. J. Control. Release Soc.* **2016**, *243*, 357–369. https://doi.org/10.1016/j.jconrel.2016.10.027.

(8) Varga, N.; Csapó, E.; Majláth, Z.; Ilisz, I.; Krizbai, I. A.; Wilhelm, I.; Knapp, L.; Toldi, J.; Vécsei, L.; Dékány, I. Targeting of the Kynurenic Acid across the Blood-Brain Barrier by Core-Shell Nanoparticles. *Eur. J. Pharm. Sci. Off. J. Eur. Fed. Pharm. Sci.* **2016**, *86*, 67–74. https://doi.org/10.1016/j.ejps.2016.02.012.

(9) Teleanu, D.; Chircov, C.; Grumezescu, A.; Volceanov, A.; Teleanu, R. Blood-Brain Delivery Methods Using Nanotechnology. *Pharmaceutics* **2018**, *10* (4), 269. https://doi.org/10.3390/pharmaceutics10040269.

(10) Oller-Salvia, B.; Sánchez-Navarro, M.; Giralt, E.; Teixidó, M. Blood–Brain Barrier Shuttle Peptides: An Emerging Paradigm for Brain Delivery. *Chem. Soc. Rev.* **2016**, *45* (17), 4690–4707. https://doi.org/10.1039/C6CS00076B.

(11) Chen, X.; Zhang, Q.; Li, B.; Lu, C.; Yang, S.; Long, J.; He, B.; Chen, H.; Huang, J. BBPpredict: A Web Service for Identifying Blood-Brain Barrier Penetrating Peptides. *Front. Genet.* **2022**, *13*, 845747. https://doi.org/10.3389/fgene.2022.845747.

(12) Malcor, J.-D.; Payrot, N.; David, M.; Faucon, A.; Abouzid, K.; Jacquot, G.; Floquet, N.; Debarbieux, F.; Rougon, G.; Martinez, J.; Khrestchatisky, M.; Vlieghe, P.; Lisowski, V. Chemical Optimization of New Ligands of the Low-Density Lipoprotein Receptor as Potential Vectors for Central Nervous System Targeting. *J. Med. Chem.* **2012**, *55* (5), 2227–2241. https://doi.org/10.1021/jm2014919.

(13) Ruan, H.; Chai, Z.; Shen, Q.; Chen, X.; Su, B.; Xie, C.; Zhan, C.; Yao, S.; Wang, H.; Zhang, M.; Ying, M.; Lu, W. A Novel Peptide Ligand RAP12 of LRP1 for Glioma Targeted Drug Delivery. *J. Controlled Release* **2018**, *279*, 306–315. https://doi.org/10.1016/j.jconrel.2018.04.035.

(14) Yin, T.; Yang, L.; Liu, Y.; Zhou, X.; Sun, J.; Liu, J. Sialic Acid (SA)-Modified Selenium Nanoparticles Coated with a High Blood–Brain Barrier Permeability Peptide-B6 Peptide for Potential Use in Alzheimer's Disease. *Acta Biomater.* **2015**, *25*, 172–183. https://doi.org/10.1016/j.actbio.2015.06.035.

(15) De Jong, E.; Williams, D. S.; Abdelmohsen, L. K. E. A.; Van Hest, J. C. M.; Zuhorn, I. S. A Filter-Free Blood-Brain Barrier Model to Quantitatively Study Transendothelial Delivery of Nanoparticles by Fluorescence Spectroscopy. *J. Controlled Release* **2018**, *289*, 14–22. https://doi.org/10.1016/j.jconrel.2018.09.015.

(16) Kumar, P.; Wu, H.; McBride, J. L.; Jung, K.-E.; Hee Kim, M.; Davidson, B. L.; Kyung Lee, S.; Shankar, P.; Manjunath, N. Transvascular Delivery of Small Interfering RNA to the Central Nervous System. *Nature* **2007**, *448* (7149), 39–43. https://doi.org/10.1038/nature05901.

(17) Demeule, M.; Currie, J.-C.; Bertrand, Y.; Ché, C.; Nguyen, T.; Régina, A.; Gabathuler, R.; Castaigne, J.-P.; Béliveau, R. Involvement of the Low-Density Lipoprotein Receptor-Related Protein in the Transcytosis of the Brain Delivery Vector Angiopep-2. *J. Neurochem.* **2008**, *106* (4), 1534–1544. https://doi.org/10.1111/j.1471-4159.2008.05492.x.

(18) Habib, S.; Singh, M. Angiopep-2-Modified Nanoparticles for Brain-Directed Delivery of Therapeutics: A Review. *Polymers* **2022**, *14* (4), 712. https://doi.org/10.3390/polym14040712.

(19) Wang, S.; Zhao, C.; Liu, P.; Wang, Z.; Ding, J.; Zhou, W. Facile Construction of Dual-Targeting Delivery System by Using Lipid Capped Polymer Nanoparticles for Anti-Glioma Therapy. *RSC Adv.* **2018**, *8* (1), 444–453. https://doi.org/10.1039/C7RA12376K.

(20) Guo, Q.; Zhu, Q.; Miao, T.; Tao, J.; Ju, X.; Sun, Z.; Li, H.; Xu, G.; Chen, H.; Han, L. LRP1-Upregulated Nanoparticles for Efficiently Conquering the Blood-Brain Barrier and Targetedly Suppressing Multifocal and Infiltrative Brain Metastases. *J. Controlled Release* **2019**, *303*, 117–129. https://doi.org/10.1016/j.jconrel.2019.04.031.

(21) Figueiredo, P.; Balasubramanian, V.; Shahbazi, M.-A.; Correia, A.; Wu, D.; Palivan, C. G.; Hirvonen, J. T.; Santos, H. A. Angiopep2-Functionalized Polymersomes for Targeted Doxorubicin Delivery to Glioblastoma Cells. *Int. J. Pharm.* **2016**, *511* (2), 794–803. https://doi.org/10.1016/j.ijpharm.2016.07.066.

(22) Luo, Z.; Jin, K.; Pang, Q.; Shen, S.; Yan, Z.; Jiang, T.; Zhu, X.; Yu, L.; Pang, Z.; Jiang, X. On-Demand Drug Release from Dual-Targeting Small Nanoparticles Triggered by High-Intensity Focused Ultrasound Enhanced Glioblastoma-Targeting Therapy. *ACS Appl. Mater. Interfaces* **2017**, *9* (37), 31612–31625. https://doi.org/10.1021/acsami.7b10866.

(23) Kim, B.-S.; Park, S. W.; Hammond, P. T. Hydrogen-Bonding Layer-by-Layer-Assembled Biodegradable Polymeric Micelles as Drug Delivery Vehicles from Surfaces. *ACS Nano* **2008**, *2* (2), 386–392. https://doi.org/10.1021/nn700408z.

(24) Correa, S.; Boehnke, N.; Deiss-Yehiely, E.; Hammond, P. T. Solution Conditions Tune and Optimize Loading of Therapeutic Polyelectrolytes into Layer-by-Layer Functionalized Liposomes. *ACS Nano* **2019**, *13* (5), 5623–5634. https://doi.org/10.1021/acsnano.9b00792.

(25) Kong, S. M.; Costa, D. F.; Jagielska, A.; Van Vliet, K. J.; Hammond, P. T. Stiffness of Targeted Layer-by-Layer Nanoparticles Impacts Elimination Half-Life, Tumor Accumulation, and Tumor Penetration. *Proc. Natl. Acad. Sci.* **2021**, *118* (42), e2104826118. https://doi.org/10.1073/pnas.2104826118.

(26) Ramasamy, T.; Haidar, Z. S.; Tran, T. H.; Choi, J. Y.; Jeong, J.-H.; Shin, B. S.; Choi, H.-G.; Yong, C. S.; Kim, J. O. Layer-by-Layer Assembly of Liposomal Nanoparticles with PEGylated Polyelectrolytes Enhances Systemic Delivery of Multiple Anticancer Drugs. *Acta Biomater.* **2014**, *10* (12), 5116–5127. https://doi.org/10.1016/j.actbio.2014.08.021.

(27) Deng, Z. J.; Morton, S. W.; Ben-Akiva, E.; Dreaden, E. C.; Shopsowitz, K. E.; Hammond, P. T. Layer-by-Layer Nanoparticles for Systemic Codelivery of an Anticancer Drug and SiRNA for Potential Triple-Negative Breast Cancer Treatment. *ACS Nano* **2013**, *7* (11), 9571–9584. https://doi.org/10.1021/nn4047925.

(28) Boehnke, N.; Dolph, K. J.; Juarez, V. M.; Lanoha, J. M.; Hammond, P. T. Electrostatic Conjugation of Nanoparticle Surfaces with Functional Peptide Motifs. *Bioconjug. Chem.* **2020**, *31* (9), 2211–2219. https://doi.org/10.1021/acs.bioconjchem.0c00384.

(29) Shen, J.; Zhan, C.; Xie, C.; Meng, Q.; Gu, B.; Li, C.; Zhang, Y.; Lu, W. Poly(Ethylene Glycol)-Block-Poly(D,L-Lactide Acid) Micelles Anchored with Angiopep-2 for Brain-Targeting Delivery. *J. Drug Target.* **2011**, *19* (3), 197–203. https://doi.org/10.3109/1061186X.2010.483517.

(30) Ruan, C.; Liu, L.; Lu, Y.; Zhang, Y.; He, X.; Chen, X.; Zhang, Y.; Chen, Q.; Guo, Q.; Sun, T.; Jiang, C. Substance P-Modified Human Serum Albumin Nanoparticles Loaded with Paclitaxel for Targeted Therapy of Glioma. *Acta Pharm. Sin. B* **2018**, *8* (1), 85–96. https://doi.org/10.1016/j.apsb.2017.09.008.

(31) Tu, Z.; Young, A.; Murphy, C.; Liang, J. F. The PH Sensitivity of Histidine-Contain- Ing Lytic Peptides: PH-SENSITIVE PEPTIDE. *J. Pept. Sci.* **2009**, *15* (11), 790–795. https://doi.org/10.1002/psc.1180.

(32) Kumthekar, P.; Tang, S.-C.; Brenner, A. J.; Kesari, S.; Piccioni, D. E.; Anders, C.; Carrillo, J.; Chalasani, P.; Kabos, P.; Puhalla, S.; Tkaczuk, K.; Garcia, A. A.; Ahluwalia, M. S.; Wefel, J. S.; Lakhani, N.; Ibrahim, N. ANG1005, a Brain-Penetrating Peptide–Drug Conjugate, Shows Activity in Patients with Breast Cancer with Leptomeningeal Carcinomatosis and Recurrent Brain Metastases. *Clin. Cancer Res.* **2020**, *26* (12), 2789–2799. https://doi.org/10.1158/1078-0432.CCR-19-3258.